

Dynamics and bifurcations of critical points of vorticity, with application to vortex merging

Morten Brøns¹ , Ilteber R. Ozdemir^{1,2} , Matthias Heil³ ,
Morten Andersen⁴  and Jesper Schmidt Hansen⁴

¹Department of Applied Mathematics and Computer Science, Technical University of Denmark, Lyngby 2800, Denmark

²Department of Mathematics, Imperial College London, London SW7 2AZ, UK

³School of Mathematics, University of Manchester, Oxford Road, Manchester M13 9PL, UK

⁴IMFUFA, Department of Science and Environment, Roskilde University, Universitetsvej 1, Roskilde 4000, Denmark

Corresponding author: Morten Brøns, mobr@dtu.dk

(Received 24 June 2024; revised 3 February 2025; accepted 20 March 2025)

The critical points of vorticity in a two-dimensional viscous flow are essential for identifying coherent structures in the vorticity field. Their bifurcations as time progresses can be associated with the creation, destruction or merging of vortices, and we analyse these processes using the equation of motion for these points. The equation decomposes the velocity of a critical point into advection with the fluid and a drift proportional to viscosity. Conditions for the drift to be small or vanish are derived, and the analysis is extended to cover bifurcations. We analyse the dynamics of vorticity extrema in numerical simulations of merging of two identical vortices at Reynolds numbers ranging from 5 to 1500 in the light of the theory. We show that different phases of the merging process can be identified on the basis of the balance between advection and drift of the critical points, and identify two types of merging, one for low and one for high values of the Reynolds number. In addition to local maxima of positive vorticity and minima of negative vorticity, which can be considered centres of vortices, minima of positive vorticity and maxima of negative vorticity can also exist. We find that such anti-vortices occur in the merging process at high Reynolds numbers, and discuss their dynamics.

Key words: vortex interactions, bifurcation, topological fluid dynamics

1. Introduction

The merging of two-dimensional identical co-rotating vortices is a complicated process. The most basic configuration for exploring vortex merging is an initial state with two isolated, identical and axisymmetric blobs of vorticity that evolve with the dynamics of the flow. A large body of experimental, computational and theoretical studies of this fundamental flow problem exists in the literature. Early research focused on the inviscid dynamics of vortex patches (Overman & Zabusky 1982; Dritschel 1985), and the main tool to study vortex merging was contour dynamics combined with contour surgery (Deem & Zabusky 1978; Dritschel 1986). For more recent work on viscous flows, see e.g. Meunier *et al.* (2002, 2005), Le Dizès & Verga (2002), Cerretelli & Williamson (2003), Josserand & Rossi (2007) and the review by Leweke *et al.* (2016).

Keeping track of the dynamics of the vortex centres, defined as the local extrema of vorticity of each of the two vortices, has proved to give useful insight into the merging process in viscous flow. From experimental data, Cerretelli & Williamson (2003) identified stages in the merging process based mainly on the distance $d(t)$ between the two vortex centres. They found that in the early stage, called the first diffusive stage, the vortices behave essentially as point vortices with a constant distance. As the vortex cores grow by diffusion and start to overlap, the dynamics enters the convective stage, where the distance between the vortex centres decreases linearly. This is followed by the second diffusive stage, where the inward motion of the vortex centres slows down markedly, before they quickly approach and merge. In the final stage, the merged diffusive stage, the vorticity organises itself into a single symmetric Gaussian vortex of decaying strength.

Several studies have contributed to our understanding of the dynamics of the distance $d(t)$. Cerretelli & Williamson (2003) show that the anti-symmetric part of vorticity in a frame co-rotating with the vortices is responsible for the radial advection of the vortices. They found experimentally that the anti-symmetric vorticity induces an inward velocity of the vortices. Brandt & Nomura (2006) and Josserand & Rossi (2007) have determined the contribution from the filaments of vorticity that develop in the merging process to $d(t)$ in the convective stage. Jing *et al.* (2012) and Andersen *et al.* (2019) have used the core growth model, shown by Nielsen *et al.* (2021) to be a good approximation to Navier–Stokes dynamics at low Reynolds numbers, to compute $d(t)$. Computational studies by Sreejith & Anil (2021) have separated the effects of advection and diffusion on $d(t)$ – an approach that we will pursue – and give a theoretical foundation for in what follows.

In the present paper, we explore the dynamics of the vortex centres further by revisiting a general equation of motion for critical points of vorticity first derived by Brøns & Bisgaard (2010). The equation holds for local extrema of vorticity, such as vortex centres, and for saddle points. The equation, (2.9) in § 2.1, expresses the velocity of a critical point of vorticity as the advection with the fluid velocity plus a drift proportional to viscosity. We will discuss conditions for the viscous drift to be small or zero, and extend the analysis to bifurcation of critical points when time is considered the bifurcation parameter. Such bifurcations correspond to the creation, destruction or merging of vortices. Both the generic case (cusp bifurcation) and the symmetric case (pitchfork bifurcation), which is relevant for merging of identical vortices, are covered. An important result is that the viscous drift velocity goes to infinity as a bifurcation is approached, and hence dominates the motion of the vortex centre no matter the fluid velocity. The bifurcations have previously been identified in the vortex dynamics in the flow behind stationary and oscillating cylinders (Heil *et al.* 2017; Nielsen *et al.* 2022) and in vortex merging, modelled by the core growth model (Andersen *et al.* 2019), but has to our knowledge not been analysed fully before.

Our analysis holds for all types of critical points of vorticity. Local maxima of positive vorticity and local minima of negative vorticity are vortex centres, but minima of positive vorticity and maxima of negative vorticity can also exist. We call such points anti-vortices, and show that in contrast to true vortices, anti-vortices gain strength as time progresses.

The equation of motion and the bifurcation analysis are of a general nature and can be applied to describe the vortex dynamics of any two-dimensional flow. We illustrate this by analysing numerical simulations of the merging of two identical vortices in the Reynolds number range from 5 to 1500. We show how the decomposition of the motion of the vortex centres into advection and viscous drift can be used to identify different phases during merging, and on this basis, identify two qualitatively different merging processes depending on the Reynolds number.

The paper is organised as follows. In § 2, we derive the equation of motion for critical points of vorticity, and discuss the physical consequences. The bifurcation analysis is performed in § 3. In § 4, we apply the theoretical results to numerical simulation of vortex merging. Conclusions are drawn in § 5.

2. Dynamics of regular critical points of vorticity

2.1. Equation of motion

Let $\mathbf{x}_c(t)$ denote a critical point of a smooth, two-dimensional unsteady vorticity field $\omega(\mathbf{x}, t)$. By definition, it fulfils

$$\nabla\omega(\mathbf{x}_c(t), t) = \mathbf{0}. \tag{2.1}$$

If the Hessian $\mathbf{H} = \nabla(\nabla\omega)$ in rectangular coordinates (x, y) given by

$$\mathbf{H} = \begin{pmatrix} \partial_{xx}\omega & \partial_{xy}\omega \\ \partial_{xy}\omega & \partial_{yy}\omega \end{pmatrix}, \tag{2.2}$$

evaluated at $\mathbf{x}_c(t)$, is regular, then the type of the critical point is determined by the sign of the determinant, $\det \mathbf{H}$. If $\det \mathbf{H} > 0$, then \mathbf{x}_c is a local extremum of vorticity; if $\det \mathbf{H} < 0$, then it is a saddle point. Local maxima of positive vorticity and local minima of negative vorticity are considered centres of vortices. The physical interpretation of saddle points is less obvious, but as we will see, they play an important topological role in the creation and destruction of vortices.

The eigenvalues λ_1, λ_2 of \mathbf{H} describe the shape of a vortex in a neighbourhood of an extremum. Close to such a point, the iso-vorticity curves are closed, and to second order in the distance, the curves are ellipses. If the half-axes are denoted a, b , then the eccentricity is

$$e = \sqrt{1 - b^2/a^2} = \sqrt{1 - \lambda_1/\lambda_2}, \tag{2.3}$$

where $|\lambda_1| \leq |\lambda_2|$ is assumed. The eccentricity is a measure of how much the shape of the vortex deviates from axisymmetry. The absolute values of the eigenvalues measure the concentration of the vortex. The larger they are, the more rapidly the magnitude of vorticity decays away from the extremum.

Implicit differentiation of (2.1) yields

$$\mathbf{H}\dot{\mathbf{x}}_c + \partial_t \nabla\omega = \mathbf{0}, \tag{2.4}$$

from which the velocity of the critical point can be found:

$$\dot{\mathbf{x}}_c = -\mathbf{H}^{-1} \partial_t \nabla\omega. \tag{2.5}$$

Further information can be obtained from the vorticity transport equation

$$\partial_t \omega = -\mathbf{u} \cdot \nabla \omega + \nu \Delta, \tag{2.6}$$

where \mathbf{u} is the underlying fluid velocity field, ν is the kinematic viscosity, and $\Delta = \nabla^2$ is the Laplacian of the vorticity. Taking the gradient on both sides of this equation, one obtains

$$\partial_t \nabla \omega = -(\nabla \mathbf{u}) \nabla \omega - \mathbf{H} \mathbf{u} + \nu \nabla \Delta. \tag{2.7}$$

Evaluating at a critical point of vorticity where $\nabla \omega = \mathbf{0}$, this reduces to

$$\partial_t \nabla \omega = -\mathbf{H} \mathbf{u} + \nu \nabla \Delta. \tag{2.8}$$

Inserting (2.8) in (2.5) then gives

$$\dot{\mathbf{x}}_c = \mathbf{u} - \nu \mathbf{H}^{-1} \nabla \Delta. \tag{2.9}$$

This equation of motion for a critical point of vorticity was first derived in rectangular coordinates by Brøns & Bisgaard (2010), but not analysed in any detail. The form (2.9) is a general, coordinate-free vector equation. It expresses the velocity of the critical point $\dot{\mathbf{x}}_c$ as the sum of the advection by the fluid $\mathbf{v}_a = \mathbf{u}$ and a viscous drift velocity $\mathbf{v}_d = -\nu \mathbf{H}^{-1} \nabla \Delta$. The viscous drift velocity is proportional to viscosity but otherwise depends only on spatial derivatives of the vorticity field, evaluated at the critical point. However, the effect of viscosity is not isolated to the viscous drift velocity. The velocity field itself satisfies the Navier–Stokes equations, hence the advection velocity \mathbf{v}_a implicitly depends on the viscosity too.

2.2. The viscous drift velocity

The viscous drift velocity obviously vanishes if the viscosity is zero. Thus in an inviscid fluid, the critical points of vorticity are material points. This also follows directly from the fact that in an inviscid fluid, vorticity is simply advected by the flow.

The viscous drift velocity is also zero if

$$\nabla \Delta = \mathbf{0} \tag{2.10}$$

at the critical point. To understand (2.10), consider a Cartesian coordinate system (x, y) centred at a critical point of vorticity, with corresponding polar coordinates (r, θ) . In this coordinate system, (2.10) becomes

$$\partial_{xxx} \omega_0 + \partial_{xyy} \omega_0 = 0, \quad \partial_{xxy} \omega_0 + \partial_{yyy} \omega_0 = 0, \tag{2.11}$$

where the subscript 0 denotes evaluation at the critical point.

We now consider a Fourier expansion of the vorticity, $\omega = \sum_{n=-\infty}^{\infty} c_n(r) e^{in\theta}$. A Taylor expansion in r then shows that the third-order derivatives of ω occur only in the terms

$$c_1 = \overline{c_{-1}} = \frac{1}{16} (\partial_{xxx} \omega_0 + \partial_{xyy} \omega_0 - i(\partial_{xxy} \omega_0 + \partial_{yyy} \omega_0)) r^3 + \mathcal{O}(r^5), \tag{2.12}$$

$$c_3 = \overline{c_{-3}} = \frac{1}{48} (\partial_{xxx} \omega_0 - 3\partial_{xyy} \omega_0 - i(3\partial_{xxy} \omega_0 - \partial_{yyy} \omega_0)) r^3 + \mathcal{O}(r^5). \tag{2.13}$$

Thus from (2.11) and (2.12), the critical point follows the flow if and only if the basic angular mode of vorticity, represented by c_1 , is zero to third order in r . In that case, (2.13) becomes

$$c_3 = \overline{c_{-3}} = \frac{1}{12} (\partial_{xxx} \omega_0 + i \partial_{yyy} \omega_0) r^3 + \mathcal{O}(r^5), \tag{2.14}$$

which in general is non-zero.

We note that (2.10) is satisfied for an axisymmetric vorticity field since all c_n with $n \neq 0$ then vanish. Interestingly, there is no connection to the eccentricity (2.3); vortices of any local shape as defined by the eccentricity may (or may not) follow the flow. We stress that (2.10) will, in general, hold at only one time instant. The acceleration of a critical point of vorticity will usually be different from the acceleration of the fluid particle on which it resides at the given time instant. In that case, (2.10) will be violated immediately. Only if (2.10) holds for an interval of time will a critical point of vorticity also be a material point.

If the eigenvalues of \mathbf{H} are numerically large, the eigenvalues of \mathbf{H}^{-1} are small, and the viscous velocity correction will also be small. That is, the more concentrated a vortex is, the closer it follows the fluid flow – for given viscosity and $\nabla\Lambda$.

The strength of a vortex measured by the value ω_0 at the extremum plays no role for its motion, as (2.9) depends only on derivatives of ω . In particular, the analysis above also holds for local maxima of negative vorticity and local minima of positive vorticity. We call such points anti-vortices. They are reminiscent of the holes inside a Q -vortex observed by Nielsen *et al.* (2021). The rate of change of vorticity at a critical point is

$$\frac{d}{dt}\omega(\mathbf{x}_c(t), t) = \nabla\omega \cdot \dot{\mathbf{x}}_c + \partial_t\omega = \nabla\omega \cdot (\dot{\mathbf{x}}_c - \mathbf{u}) + \nu\Lambda = \nu\Lambda, \tag{2.15}$$

where we used the vorticity transport equation (2.6) and the definition (2.1) of a critical point. Since $\Lambda = \text{tr}(\mathbf{H})$, it follows that vorticity decreases for a maximum of vorticity and increases for a minimum of vorticity. Hence an anti-vortex will preserve its type, whereas a vortex can turn into an anti-vortex as time progresses. For saddle points, Λ can have either sign.

3. Bifurcation of critical points of vorticity

3.1. The generic case

As long as \mathbf{H} is regular at a critical point of vorticity, the point will move according to (2.9), and the type of the point (extremum or saddle) will not change. If, however, at some time instant, \mathbf{H} becomes singular, then a local bifurcation event is expected, as the velocity of the critical point is no longer well-defined from (2.4). Here, we consider the case where \mathbf{H} attains a simple zero eigenvalue at $t = 0$. We choose the coordinate system such that the critical point is at the origin, and \mathbf{H} is diagonal. The Hessian then has a simple zero eigenvalue exactly when one of $\partial_{xx}\omega$ and $\partial_{yy}\omega$ is zero. Here, we assume

$$\partial_{xy}\omega_0 = 0, \quad \partial_{xx}\omega_0 = 0, \quad \partial_{yy}\omega_0 \neq 0, \tag{3.1}$$

where the subscript 0 here and in the following indicates evaluation at $(x, y, t) = (0, 0, 0)$, so any quantities with a subscript 0 are constants. Specifically, we have

$$\mathbf{H}_0 = \begin{pmatrix} 0 & 0 \\ 0 & \partial_{yy}\omega_0 \end{pmatrix}, \tag{3.2}$$

and since \mathbf{H}_0 is singular, it is not possible to solve $\nabla\omega(x, y, t) = \mathbf{0}$ for x, y with the implicit function theorem as in § 2.1. However, assuming for now the non-degeneracy condition

$$\nu \partial_x \Lambda_0 \neq 0, \tag{3.3}$$

the equation can be solved for y, t since the Jacobian matrix

$$\mathbf{J}_0 = \frac{\partial(\partial_x\omega, \partial_y\omega)}{\partial(y, t)} \Big|_0 = \begin{pmatrix} \partial_{xy}\omega_0 & \partial_{xt}\omega_0 \\ \partial_{yy}\omega_0 & \partial_{yt}\omega_0 \end{pmatrix} = \begin{pmatrix} 0 & \nu \partial_x \Lambda_0 \\ \partial_{yy}\omega_0 & -\partial_{yy}\omega_0 v_0 + \nu \partial_y \Lambda_0 \end{pmatrix} \tag{3.4}$$

is then regular. In § 3.2, we consider a symmetric flow where (3.3) is violated. The expressions in the last column of the last matrix follow from (2.8), using that $\mathbf{H}_0 \mathbf{u}_0 = (0, \partial_{yy} \omega_0 v_0)^T$, where $\mathbf{u}_0 = (u_0, v_0)^T$ is the velocity at the origin. Thus it follows from the implicit function theorem that there exist functions $y = y^*(x)$, $t = t^*(x)$ defined for x close to 0 with $y^*(0) = 0$, $t^*(0) = 0$ such that

$$\partial_x \omega(x, y^*(x), t^*(x)) = 0, \quad \partial_y \omega(x, y^*(x), t^*(x)) = 0. \tag{3.5}$$

Derivatives of y^* , t^* at $x = 0$ can be found by repeated differentiation of (3.5), the first two orders being

$$\begin{pmatrix} y^{*'}(0) \\ t^{*'}(0) \end{pmatrix} = -\mathbf{J}_0^{-1} \begin{pmatrix} \partial_{xx} \omega_0 \\ \partial_{xy} \omega_0 \end{pmatrix} = \begin{pmatrix} 0 \\ 0 \end{pmatrix} \tag{3.6}$$

and

$$\begin{pmatrix} y^{*''}(0) \\ t^{*''}(0) \end{pmatrix} = -\mathbf{J}_0^{-1} \begin{pmatrix} \partial_{xxx} \omega_0 \\ \partial_{xxy} \omega_0 \end{pmatrix} = \begin{pmatrix} -\frac{\partial_{xxx} \omega_0 v_0}{v \partial_x \Lambda_0} + \frac{\partial_{xxx} \omega_0 \partial_y \Lambda_0 - \partial_{xxy} \omega_0 \partial_x \Lambda_0}{\partial_{yy} \omega_0 \partial_x \Lambda_0} \\ -\frac{\partial_{xxx} \omega_0}{v \partial_x \Lambda_0} \end{pmatrix}, \tag{3.7}$$

where (3.1) has been used. A Taylor expansion yields

$$y^*(x) = \frac{y^{*''}(0)}{2} x^2 + \mathcal{O}(x^3), \quad t^*(x) = \frac{t^{*''}(0)}{2} x^2 + \mathcal{O}(x^3), \tag{3.8}$$

and further assuming the non-degeneracy condition

$$\partial_{xxx} \omega_0 \neq 0, \tag{3.9}$$

it follows that $t^{*''}(0) \neq 0$ such that (3.8) can be solved to yield trajectories of critical points:

$$x_c(t) = \pm \sqrt{\frac{2t}{t^{*''}(0)}} + \mathcal{O}(t), \quad y_c(t) = \frac{y^{*''}(0)}{t^{*''}(0)} t + \mathcal{O}(t^{3/2}). \tag{3.10}$$

The dominating terms can be found from (3.7). For $x_c(t)$, it is interesting to resolve the $\mathcal{O}(t)$ term, which requires finding $t^{*'''}(0)$. We omit the tedious computations and only state the final result:

$$\begin{aligned} x_c(t) &= \pm \sqrt{-2v \frac{\partial_x \Lambda_0}{\partial_{xxx} \omega_0} t} \\ &+ \left(u_0 + v \left[\frac{\partial_{xxx} \omega_0 \partial_{xxy} \omega_0 \partial_y \Lambda_0 - \partial_{xxy} \omega_0^2 \partial_x \Lambda_0}{\partial_{xxx} \omega_0^2 \partial_{yy} \omega_0} + \frac{\partial_{xxx} \omega_0 \partial_x \Lambda_0 - 3 \partial_{xxx} \omega_0 \partial_{xx} \Lambda_0}{3 \partial_{xxx} \omega_0^2} \right] \right) t \\ &+ \mathcal{O}(t^{3/2}), \end{aligned} \tag{3.11a}$$

$$y_c(t) = \left(v_0 + v \frac{\partial_{xxy} \omega_0 \partial_x \Lambda_0 - \partial_{xxx} \omega_0 \partial_y \Lambda_0}{\partial_{yy} \omega_0 \partial_{xxx} \omega_0} \right) t + \mathcal{O}(t^{3/2}). \tag{3.11b}$$

If $\partial_x \Lambda_0 / \partial_{xxx} \omega_0 > 0$, then two critical points exist for $t < 0$, one for each sign of $x_c(t)$; these merge and disappear at the origin at $t = 0$. If $\partial_x \Lambda_0 / \partial_{xxx} \omega_0 < 0$, then two critical points are created at $t = 0$ and exist for $t > 0$. The types of the critical points are found from the eigenvalues of the Hessian

$$\mathbf{H}(x, y^*(x), t^*(x)) = \begin{pmatrix} \partial_{xxx} \omega_0 x + \mathcal{O}(x^2) & \mathcal{O}(x) \\ \mathcal{O}(x) & \partial_{yy} \omega_0 + \mathcal{O}(x) \end{pmatrix}. \tag{3.12}$$

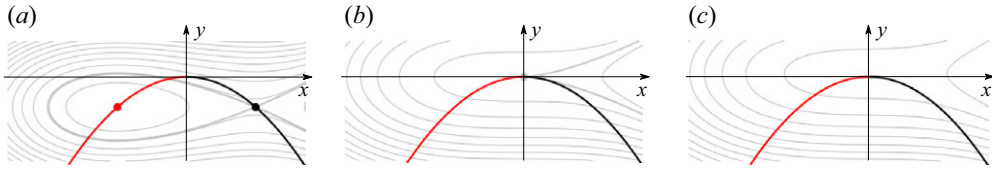


Figure 1. Illustration of annihilation of critical points in a cusp bifurcation. The grey curves are iso-lines of vorticity. The red (black) point is the extremum (saddle point) of vorticity, and the red and black curves are the corresponding trajectories: (a) before bifurcation; (b) at the bifurcation point; (c) after bifurcation. For critical point creation, the temporal order is reversed.

The eigenvalues are $\lambda_1 = \partial_{xxx}\omega_0 x + O(x^2)$ and $\lambda_2 = \partial_{yy}\omega_0 + O(x)$. Since $x > 0$ for one critical point and $x < 0$ for the other, one point is an extremum, and the other is a saddle.

The bifurcation is therefore a cusp or a saddle–centre bifurcation, and it is illustrated in figure 1. The sequence (a) \rightarrow (b) \rightarrow (c) shows the merging of an extremum and a saddle. The critical points follow each of the two branches of a locally parabolic trajectory for $t < 0$ (figure 1a), coalesce into a degenerate critical point at $t = 0$ (figure 1b), and then disappear for $t > 0$ (figure 1c).

The bifurcation occurs in viscous flows only, as the second condition in (3.3) requires $\nu \neq 0$. In inviscid flow, critical points of vorticity never merge, and no new ones are created.

The terms linear in t in (3.11) have the same structure as in the regular case (2.9); the velocity of a critical point is the sum of an advection with the fluid and a drift velocity proportional to viscosity. For the motion in the y -direction, the linear term is dominating near the bifurcation, but in the x -direction, the leading-order term of the position is of order $t^{1/2}$, which leads to a velocity that goes to infinity as $|t|^{-1/2}$ when the bifurcation is approached. Hence the viscous drift dominates the motion of the critical points completely, no matter the fluid velocity. That viscous drift must be present near the bifurcation is already clear from (3.3). It implies that $\nabla \Lambda_0 \neq \mathbf{0}$, hence violating (2.10) for zero viscous drift.

The eccentricity (2.3) of the level curves of vorticity close to the extremum of vorticity when the bifurcation is approached is

$$e = \sqrt{1 - \frac{\partial_{xxx}\omega_0}{\partial_{yy}\omega_0} x + O(x^2)} \approx 1 - \frac{\partial_{xxx}\omega_0}{2\partial_{yy}\omega_0} x \approx 1 - \sqrt{\frac{\nu}{2} \frac{|\partial_{xxx}\omega_0 \partial_x \Lambda_0|}{(\partial_{yy}\omega_0)^2}} \sqrt{|t|}, \quad (3.13)$$

where we used (3.11a) in the last step. This is consistent with the plot of the vortex annihilation shown in figure 1. The almost elliptic iso-vorticity curves close to the extremum are squeezed together in the y -direction faster than they shrink in the x -direction, as measured by the eccentricity, which tends to the largest possible value 1 as $t \rightarrow 0$.

3.2. Symmetric bifurcation

If two vortices with identical distribution of vorticity are placed symmetrically around the origin in a Cartesian coordinate system, then the symmetry

$$\omega(-x, -y) = \omega(x, y) \quad (3.14)$$

will be fulfilled for the total vorticity of the two distributions. As the flow evolves, the symmetry will be preserved such that (3.14) holds for all times. This implies that all odd-order spatial derivatives at the origin are zero, and it follows that the origin is always a critical point of vorticity. If the Hessian at the origin is singular at some time instant, then

a bifurcation event is expected. However, the analysis of § 3.1 does not apply; the non-degeneracy condition (3.3) is violated since $\partial_x \Lambda_0$ is a sum of third-order derivatives of ω . Here, we therefore derive the bifurcation structure under the symmetry (3.14), which we use to study the merging of two identical vortices in § 4. We omit some details as the analysis to a large extent follows that of § 3.1.

We consider a coordinate system such that the Hessian at the origin is singular and diagonal at $t = 0$ under the assumptions (3.1), yielding the Hessian

$$H(0, 0, t) = \begin{pmatrix} \partial_{xx} \omega_0 t + \mathcal{O}(t^2) & \partial_{xy} \omega_0 t + \mathcal{O}(t^2) \\ \partial_{xy} \omega_0 t + \mathcal{O}(t^2) & \partial_{yy} \omega_0 + \mathcal{O}(t) \end{pmatrix}. \tag{3.15}$$

Furthermore, we assume the non-degeneracy condition

$$\partial_{xx} \omega_0 = \nu \partial_{xx} \Lambda_0 \neq 0, \tag{3.16}$$

where the identity is obtained by differentiation of (2.8). As before, the subscript indicates evaluation at the bifurcation point $(x, y, t) = (0, 0, 0)$. It follows that

$$\det H(0, 0, t) = \nu \partial_{xx} \Lambda_0 \partial_{yy} \omega_0 t + \mathcal{O}(t^2), \tag{3.17}$$

such that the critical point at the origin changes between an extremum and a saddle at $t = 0$.

We introduce a new variable η by $y = \eta x$, and define

$$\tilde{f}(x, \eta, t) = \partial_x \omega(x, \eta x, t), \quad \tilde{g}(x, \eta, t) = \partial_y \omega(x, \eta x, t), \tag{3.18}$$

and note that $\tilde{f}(0, \eta, t) = \tilde{g}(0, \eta, t) = 0$ for all η, t . It follows that x is a factor in both \tilde{f} and \tilde{g} , and that critical points of vorticity other than the origin can be found from

$$f(x, \eta, t) = \tilde{f}(x, \eta, t)/x = 0, \quad g(x, \eta, t) = \tilde{g}(x, \eta, t)/x = 0. \tag{3.19}$$

Consider the Jacobian

$$J_0 = \frac{\partial(f, g)}{\partial(\eta, t)} \Big|_0 = \begin{pmatrix} 0 & \partial_{xx} \omega_0 \\ \partial_{yy} \omega_0 & \partial_{xy} \omega_0 \end{pmatrix} = \begin{pmatrix} 0 & \nu \partial_{xx} \Lambda_0 \\ \partial_{yy} \omega_0 & -\partial_{yy} \omega_0 \partial_x v_0 + \nu \partial_{xy} \Lambda_0 \end{pmatrix}, \tag{3.20}$$

where $\partial_{xy} \omega_0$ is obtained by differentiation of (2.8). Since J_0 is regular, it follows from the implicit function theorem that there exist functions $\eta = \eta^*(x)$, $t = t^*(x)$ defined for x close to 0, with $\eta^*(0) = 0$, $t^*(0) = 0$, such that

$$f(x, \eta^*(x), t^*(x)) = 0, \quad g(x, \eta^*(x), t^*(x)) = 0. \tag{3.21}$$

By implicit differentiation of (3.21), one finds

$$\begin{aligned} \eta^{*'}(0) &= 0, & \eta^{*''}(0) &= -\frac{\partial_{xxxx} \omega_0 \partial_x v_0}{3\nu \partial_{xx} \Lambda_0} + \frac{\partial_{xxxx} \omega_0 \partial_{xy} \Lambda_0 - \partial_{xxx} \omega_0 \partial_{xx} \Lambda_0}{3\partial_{yy} \omega_0 \partial_{xx} \Lambda_0}, \\ t^{*'}(0) &= 0, & t^{*''}(0) &= -\frac{\partial_{xxxx} \omega_0}{3\nu \partial_{xx} \Lambda_0}. \end{aligned} \tag{3.22}$$

Adding the non-degeneracy condition

$$\partial_{xxxx} \omega_0 \neq 0, \tag{3.23}$$

the Taylor expansion $t = t^{*''}(0) x^2/2 + \mathcal{O}(x^3)$ can be solved for x , and inserting the solution into $y = \eta x = \eta^{*''}(0) x^3/2 + \mathcal{O}(x^4)$ yields trajectories of two critical points:

$$x_c(t) = \pm \sqrt{-6\nu \frac{\partial_{xx} \Lambda_0}{\partial_{xxxx} \omega_0} t + \mathcal{O}(t)}, \quad y_c(t) = \pm \frac{1}{2} \eta^{*''}(0) \left(-6\nu \frac{\partial_{xx} \Lambda_0}{\partial_{xxxx} \omega_0} t \right)^{3/2} + \mathcal{O}(t^2). \tag{3.24}$$

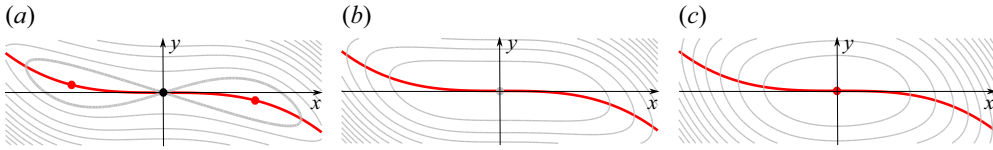


Figure 2. Illustration of the final phase of merging of identical vortices in a pitchfork bifurcation. The grey curves are iso-lines of vorticity. The red (black) points are the extrema (saddle points) of vorticity, and the red curve is the trajectory of the two extrema. (a) Before bifurcation: the heavy grey curve is the separatrix loop associated with the saddle point. (b) At the bifurcation point: the critical points coalesce at the origin. (c) After bifurcation: a single extremum remains at the origin.

The two non-degeneracy conditions (3.16) and (3.23) will be fulfilled generically if no further symmetries or similar constraints are imposed. In the case that $\partial_{yy}\omega_0$, $\partial_{xx}\Lambda_0$ and $\partial_{xxxx}\omega_0$ all have the same sign, it follows from (3.17) that the origin changes from a saddle to an extremum at $t = 0$. A simple computation shows that the critical points (3.24) that exist for $t < 0$ are both extrema. Hence the bifurcation is a supercritical pitchfork that describes the merging of two vortices as illustrated in figure 2.

If (r, θ) are polar coordinates for one of the extrema, then (3.24) yields

$$r^2 = \left| 6\nu \frac{\partial_{xx}\Lambda_0}{\partial_{xxxx}\omega_0} t \right| + \mathcal{O}(t^{3/2}), \quad \theta = \left| 3\eta^{*''}(0) \nu \frac{\partial_{xx}\Lambda_0}{\partial_{xxxx}\omega_0} t \right| + \mathcal{O}(t^{3/2}). \quad (3.25)$$

In analogy with the generic case of § 3.1, it follows that the radial velocity \dot{r} of the extrema scales as $|t|^{-1/2}$. The angular velocity of the line connecting the two extrema scales as a constant as the bifurcation is approached.

4. Application: merging of identical vortices

To illustrate our theoretical results, we consider the merging of two identical Gaussian vortices, initially centred at $(\pm d/2, 0)$. We study the evolution of these vortices in a finite domain $S = \{(x, y) \mid -L/2 \leq x, y \leq L/2\}$, where $L \gg d$, and characterise the strength of the vortices by the quantity

$$\Gamma_0 = \iint_S |\omega_0| \, dx \, dy, \quad (4.1)$$

where ω_0 is the vorticity field at the initial time $t = t_0$, both of which are specified below.

We non-dimensionalise the variables as $(x^*, y^*) = (x, y)/d$, $t^* = t\Gamma_0/d^2$, $\omega^* = \omega d^2/\Gamma_0$, $(u^*, v^*) = (u, v) d/\Gamma_0$, $\psi^* = \psi/\Gamma_0$. The flow is then governed by the non-dimensional vorticity transport equations

$$\partial_{t^*}\omega^* = -\mathbf{u}^* \cdot \nabla \omega^* + \frac{1}{2Re} \Delta \omega^*, \quad \Delta \psi^* = -\omega^*, \quad u^* = \partial_{y^*}\psi^*, \quad v^* = -\partial_{x^*}\psi^*, \quad (4.2)$$

where the Reynolds number is defined as $Re = \Gamma_0/(2\nu)$ for consistency with previous work (e.g. Meunier *et al.* 2002; Andersen *et al.* 2019). For ease of notation, we now drop the asterisks, so the variables appearing in the rest of the paper are assumed to be non-dimensional.

In the numerical simulations described below, we impose periodic boundary conditions. This requires that the integral of the vorticity over the domain vanishes, i.e. $\iint_S \omega \, dx \, dy = 0$, for all times. We therefore imposed the initial condition

$$\begin{aligned} \omega_0 &= \omega(x, y, t = t_0) \\ &= \frac{1}{2\pi\sigma_0^2} \left[\exp\left(-\frac{(x - 1/2)^2 + y^2}{\sigma_0^2}\right) + \exp\left(-\frac{(x + 1/2)^2 + y^2}{\sigma_0^2}\right) \right] - C, \end{aligned} \quad (4.3)$$

where the first term represents the two Gaussian vortices; the constant C represents a constant background vorticity, chosen such that the integral of ω_0 over S vanishes. Since the initial size of the vortices is determined by the parameter σ_0 , we choose $\sigma_0 \ll d/L \ll 1$, in which case $C \approx (d/L)^2 \ll 1$.

4.1. Numerical method

We solved the vorticity transport equation (4.2) numerically using a forward time centred space algorithm (E & Liu 1996a,b; Andersen *et al.* 2019), keeping the time step well below the von Neumann stability criterion. The Poisson equation was solved using a sparse linear equation solver (Hansen 2011; Eaton *et al.* 2021). We validated the accuracy of the scheme by repeating the simulation for the largest Reynolds number ($Re = 1500$) against a central difference scheme using a fourth-order Runge–Kutta integrator. Computations were performed on a square grid with 500×500 grid points, using domain size $L/d = 5$. When imposing the initial condition (4.3), we used $\sigma_0 = 0.015$, to ensure that the initial vorticity field resembles that associated with two point vortices. Tests on a finer grid show that the initial condition is sufficiently resolved to ensure grid-independent results. The initial time t_0 was set using the approach of Josserand & Rossi (2007), who determined t_0 such that $t = 0$ corresponds to the time when the isolated Gaussian vortices in (4.3) would have zero core radius. On the overall time scale of the vortex merging process, this is so small that the difference from choosing $t_0 = 0$ is negligible.

Given the results of the simulations, we determined the critical points of vorticity (where $\nabla\omega = \mathbf{0}$) as the intersections of the iso-contour lines $\partial_x\omega = 0$ and $\partial_y\omega = 0$. All spatial derivative calculations were performed using a fourth-order centred finite difference operator. The vorticity, the Hessian and $\nabla\Lambda$ were found at the critical points by a two-dimensional cubic interpolation scheme. The velocity of the critical points was predicted at each time step using these quantities and (2.9).

We captured the motion of the critical points by tracking their pathlines, and calculated the velocity of a critical point by using a fourth-order centred finite difference operator. Figure 3(a) shows the trajectories of the vortex centres for the case $Re = 1500$. We obtained perfect agreement between the velocity calculated from the trajectories and that predicted by (2.9), thus validating both the equation of motion and the numerical discretisation schemes used.

4.2. Numerical results

Figure 3(b) shows the quantities that we will consider in the following: the distance $d(t)$ between the vortex centres, the angle $\theta(t)$ between the line connecting the vortex centres and the x -axis, and the velocity $\dot{\mathbf{x}}_c$ of a critical point decomposed into its radial and azimuthal components, $\dot{\mathbf{x}}_c = v_r\mathbf{e}_r + v_\theta\mathbf{e}_\theta = \dot{r}\mathbf{e}_r + r\dot{\theta}\mathbf{e}_\theta$.

Figure 4 shows the distance $d(t)$ as a function of time t for a range of Reynolds numbers Re . A common feature for all Re is that initially $d(t)$ is almost constant. This can be understood from a visual inspection of the vorticity field, which shows that the vortices are highly concentrated and almost axisymmetric. The axisymmetry implies that the anti-symmetric vorticity field in the co-rotating frame is vanishing, hence there is almost no radial advection. As discussed in § 2.2, the axisymmetry and the high concentration of vorticity both imply that the viscous drift is also small, and hence that the total radial

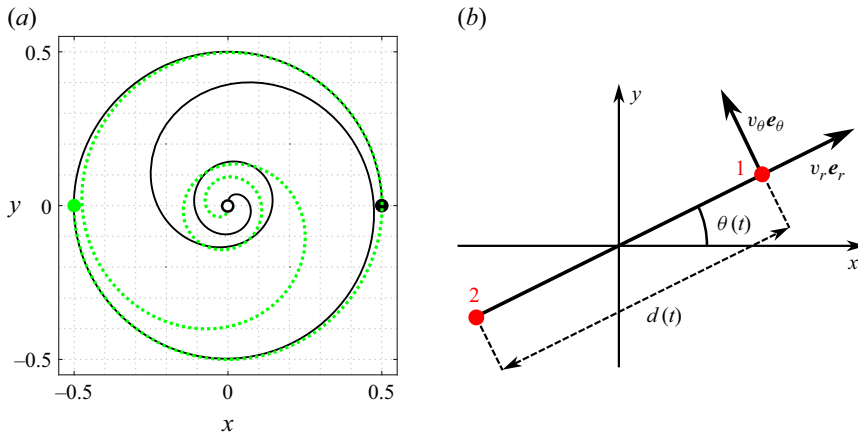


Figure 3. (a) Trajectories of vortex centres for $Re = 1500$ with initial positions $(1/2, 0)$ (black) and $(-1/2, 0)$ (dotted green). The initial positions are marked with filled circles. The open circle marks the origin, where the merging occurs. The motion is anticlockwise. (b) Instantaneous positions of vortex centres of identical vortices 1, 2 (red) with definitions of distance $d(t)$, angle $\theta(t)$ and polar decomposition (v_r, v_θ) of the velocity of vortex centre 1.

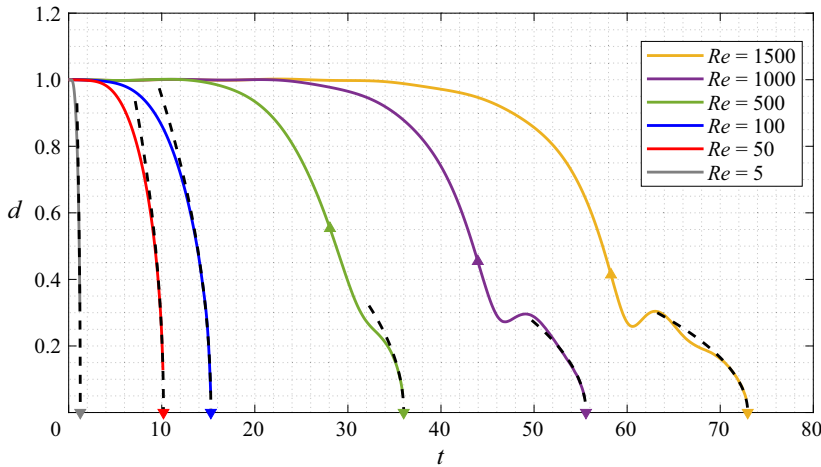


Figure 4. Distance $d(t)$ between the vortex centres during vortex merging. Scaling from (4.4) close to the bifurcation is shown as dashed black lines. Merging times are shown as inverted triangles. The upright triangles mark the inflection points.

velocity of the critical points is initially small. Another common feature is the final behaviour as merging is approached. Here, the motion is completely dominated by viscous drift according to the bifurcation analysis in § 3.2. The theory predicts, from (3.25), a scaling

$$d(t)^2 = -a_d t + b_d \tag{4.4}$$

close to merging, where

$$a_d = \frac{12}{Re} \left| \frac{\partial_{xx} \Lambda_0}{\partial_{xxxx} \omega_0} \right|, \quad b_d = \frac{12}{Re} \left| \frac{\partial_{xx} \Lambda_0}{\partial_{xxxx} \omega_0} \right| t_m, \tag{4.5}$$

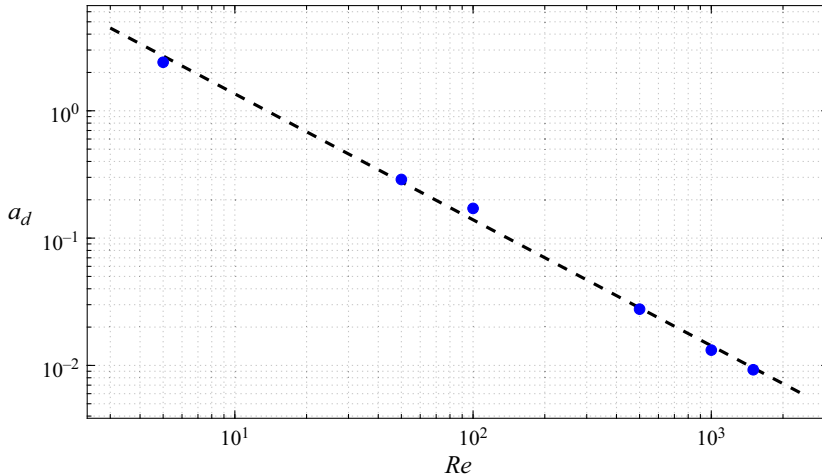


Figure 5. Scaling coefficient a_d in (4.4) as a function of Re . The dashed line is a least squares linear fit $\ln(a) = -0.989 \ln(Re) + 2.584$.

with t_m denoting the time of merging (bifurcation). Note that the coordinate system used here is that of § 3.2, which is aligned with the eigenvectors of $\mathbf{H}_0 = \mathbf{H}(0, 0, 0)$ as shown in figure 2, and not the computational frame of figure 3; the two systems differ by a rotation around the origin.

We determine t_m by interpolation as the time where the Hessian $\mathbf{H}(0, 0, t)$ has a zero eigenvalue. The merging times are marked with inverted triangles in figure 4. Computing a_d, b_d in the rotated coordinate system yields for (4.4) the dashed lines in figure 4. The very good agreement between the scaling and the simulation data confirms the theory.

Figure 5 shows that the dependence of a_d on Re is well described by the relation

$$a_d = 13.25 Re^{-0.989}, \tag{4.6}$$

i.e. a_d is essentially inversely proportional to Re . Comparing with (4.5) suggests that, at least for this flow, $\partial_{xx} \Lambda_0 / \partial_{xxxx} \omega_0$ is independent of Re .

Figure 6 shows the radial velocity v_r of vortex centre 1, decomposed into its radial advection velocity $v_{r,a}$ and its radial viscous drift velocity $v_{r,d}$ according to (2.9). Again, there are common features for all Re . The radial advective velocity $v_{r,a}$ decreases monotonically from zero (with some minor initial oscillations for higher Re) until a minimum is reached. Subsequently, $v_{r,a}$ approaches zero again, monotonically for lower Re , and with damped oscillations for higher Re . We term the time where the global minimum of $v_{r,a}$ is reached the time of maximal inward advection t_a . The radial drift velocity $v_{r,d}$ initially increases from zero to reach a small positive maximum. The viscous drift subsequently decreases to negative values, again possibly with some oscillations, and finally goes monotonically to $-\infty$ as the merging time t_m is approached. We term the time when the global maximum of $v_{r,d}$ is reached the time of maximal outward drift t_d .

The dependence of the key time instants t_a and t_d on Re relative to the merging time t_m is shown in figure 7. In general, $t_d < t_a$. At low Re , t_d/t_m is much smaller than t_a/t_m , but as Re increases, the interval between the times become shorter. The fact that in the high- Re range, t_a and t_d approach each other, is closely related to the development of an inflection point for $d(t)$ that occurs at time instant t_i , where $\dot{d}(t_i) = 0$. Such inflection points appear in figure 4 for $Re = 500$ and above. To see the connection, consider the second-order Taylor expansions of $v_{r,a}$ and $v_{r,d}$ based at t_a and t_d , respectively:

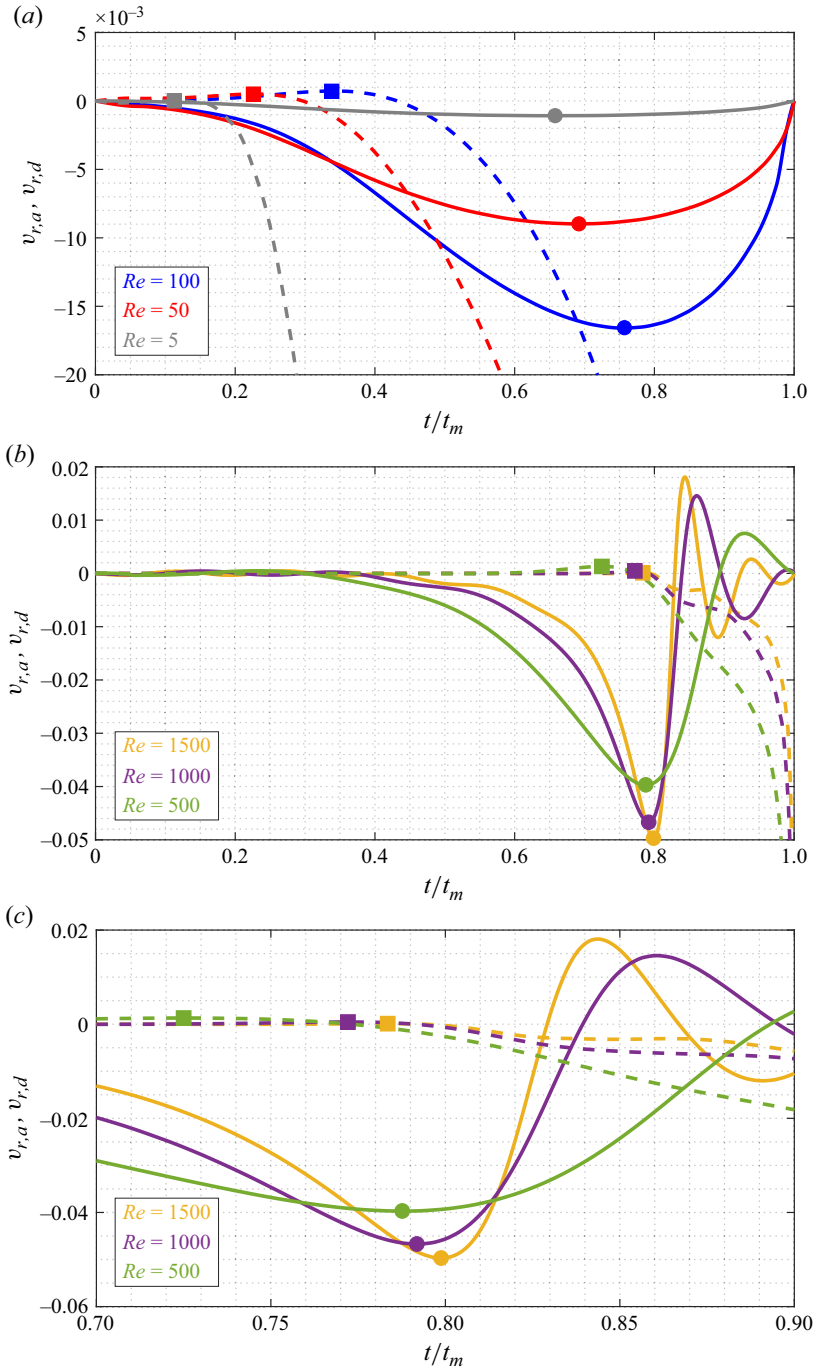


Figure 6. Radial advection velocity $v_{r,a}$ (solid lines) and radial viscous drift velocity $v_{r,d}$ (dashed lines) of vortex centre 1. Time of maximal inward advection t_a is marked with circles. Time of maximal outward drift t_d is marked with squares. Time is shown relative to the merging time t_m : (a) low Re , (b) high Re , (c) zoom of (b) near t_a and t_d .

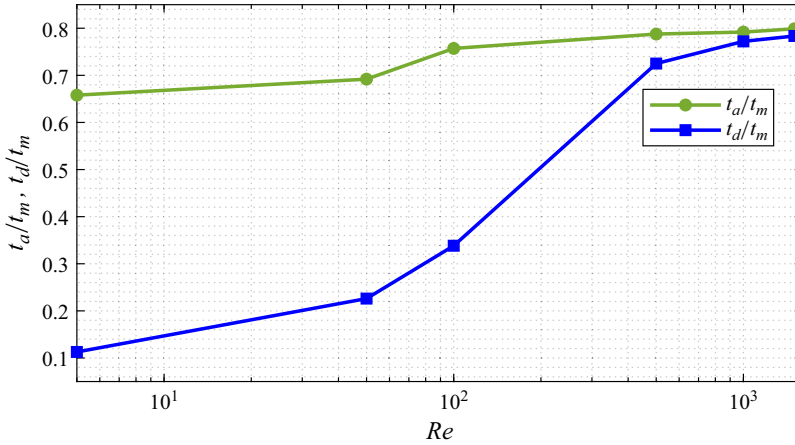


Figure 7. Relative time of maximal inward advection t_a/t_m , and relative time of maximal outward drift t_d/t_m , versus the Reynolds number.

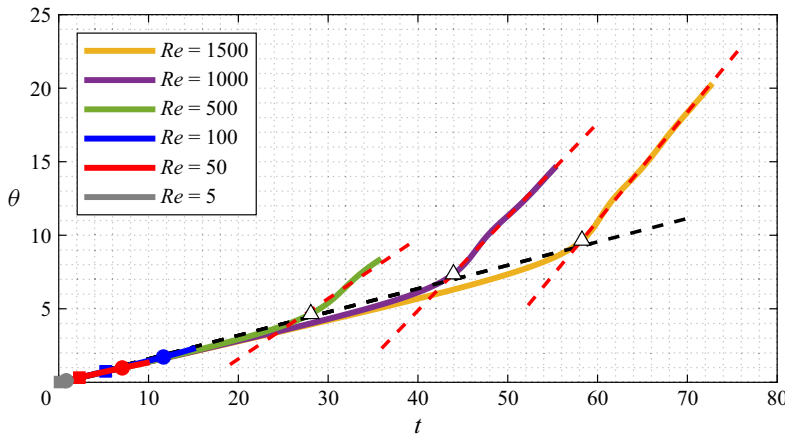


Figure 8. Angle θ of the line connecting the two vortices. The black dashed line shows the evolution for point vortices according to (4.10). The red dashed lines are expressions (4.11). The triangles mark the inflection times t_i at $Re = 500, 100, 1500$.

$$v_{r,a}(t) \approx v_{r,a}(t_a) + \frac{1}{2} \ddot{v}_{r,a}(t_a) (t - t_a)^2, \quad (4.7)$$

$$v_{r,d}(t) \approx v_{r,d}(t_d) + \frac{1}{2} \ddot{v}_{r,d}(t_d) (t - t_d)^2. \quad (4.8)$$

Both are valid simultaneously when t_a and t_d are close. Since $\ddot{d}(t) = 2(\dot{v}_{r,a}(t) + \dot{v}_{r,d}(t))$, one finds from (4.7) and (4.8) that $\ddot{d}(t) = 0$ is solved by a weighted average of t_a and t_d :

$$t_i \approx \frac{\ddot{v}_{r,a}(t_a) t_a + \ddot{v}_{r,d}(t_d) t_d}{\ddot{v}_{r,a}(t_a) + \ddot{v}_{r,d}(t_d)}. \quad (4.9)$$

It appears from figure 6(c) that $|\ddot{v}_{r,d}(t_d)| \ll |\ddot{v}_{r,a}(t_a)|$, and it follows that t_i is located between t_d and t_a .

We now turn to the evolution of the angle θ of the line connecting the two vortex centres. The results are shown in figure 8. Two point vortices with unit distance, each of circulation $1/2$, give rise to a constant angular velocity such that

$$\theta = \frac{1}{2\pi}t, \tag{4.10}$$

independent of Re . It appears from [figure 8](#) that this describes the initial dynamics well for all Re .

As the bifurcation is approached, the scaling (3.25) also implies a constant angular velocity, but now depending on Re . Inserting (3.22) into (3.25), an expression of the form

$$\theta = a_\theta t + b_\theta, \tag{4.11}$$

analogous to (4.4), can be derived. Similar to (4.5), a_θ and b_θ depend on derivatives of the flow field evaluated at the bifurcation point in a complicated way. The relation (4.11) is shown as red dashed lines in [figure 8](#) for the higher Re , where they deviate significantly from the point vortex scaling (4.10); it appears that the theoretical result agrees very well with the simulations. It is interesting that at high Re , the transition from the initial scaling (4.10) to the bifurcation scaling (4.11) takes place over a very narrow time interval around t_i that is defined solely by the properties of the radial velocity.

A decomposition of the angular velocity into advection and viscous drift, $\dot{\theta} = \dot{\theta}_a + \dot{\theta}_d$, shows that $\dot{\theta}_a$ is generally two orders of magnitude larger than $\dot{\theta}_d$. Hence advection completely dominates the rotation of the vortex pair.

4.3. Phases of the merging process

We summarise the results of §4.2 by describing the merging process as consisting of a series of phases. Each phase has a characteristic balance between advection $v_{r,a}$ and viscous drift $v_{r,d}$. We use the term ‘phases’ to avoid confusion with the ‘stages’ defined by Cerretelli & Williamson (2003) on the basis of the dynamics of $d(t)$.

The initial constant phase is characterised by both advection and viscous drift being small, which results in $d(t)$ being almost constant. The final bifurcation phase is characterised by viscous drift being dominating as $v_{r,d} \rightarrow -\infty$ for $t \rightarrow t_m$ with $d(t)$ following the scaling (4.4).

For Re up to 100, where t_d is much smaller than t_a (see [figure 7](#)), the constant phase blends smoothly into the bifurcation phase before any significant advection has occurred; see [figure 6\(a\)](#).

For $Re = 500$ and above, where t_d is close to t_a and an inflection time t_i exists, there is sufficient time for inward advection to grow while viscous drift is still negligible. This gives rise to an advective phase where the vortex centres move inwards due to advection. The constant phase now blends into the advective phase, and while we do not define a specific time instant where it starts, we formally define that the phase ends at t_a , where $v_{r,a}$ starts damped oscillations; see [figures 6\(b,c\)](#). The oscillations of $v_{r,a}$ persist until merging, and as long as the viscous drift is not too large, oscillations of $d(t)$ ensue. We term the phase after t_a where $d(t)$ oscillates the oscillatory phase, which continues until the monotonically decreasing viscous drift ultimately dominates, and the bifurcation phase is entered.

An overview of the phases and the resulting dynamics is shown in [table 1](#). The last column shows the angular velocity $\dot{\theta}$ during each phase, according to the results shown in [figure 8](#).

We note that in their experiments at $Re = 530$, Cerretelli & Williamson (2003) also observed an early constant phase, termed the first diffusive stage, which after a well-defined transition was followed by a regime termed the convective stage, where $d(t)$ varies linearly with t . This is in contrast to our results, where $d(t)$ varies smoothly as

Phase	Characterisation	Distance	Angular velocity
Constant	$ v_{r,a} \ll 1, v_{r,d} \ll 1$	$d(t) \approx 1$	$\dot{\theta} \approx \frac{1}{2\pi}$
Advective (high Re only)	$ v_{r,a} \gg v_{r,d} $	$d(t)$ decreases monotonically	$\dot{\theta} \approx \frac{1}{2\pi}$
Oscillatory (high Re only)	$v_{r,a}$ oscillates, $ v_{r,a} > v_{r,d} $	$d(t)$ oscillates	$\dot{\theta} \approx a_\theta > \frac{1}{2\pi}$
Bifurcation	$v_{r,a} \rightarrow 0, v_{r,d} \rightarrow -\infty$	$d(t)^2 \approx -a_d t + b_d$	$\dot{\theta} \approx a_\theta \geq \frac{1}{2\pi}$

Table 1. Overview of merging phases, classified by the variation of advection and viscous drift.

advection builds up. Similar smooth development of $d(t)$ is observed in the simulations by Josserand & Rossi (2007) and Sreejith & Anil (2021). However, it is interesting to note that the occurrence of an inflection point in $d(t)$ at the beginning of what we defined as the oscillatory phase implies the existence of a regime where $d(t) = d(t_i) + \dot{d}(t_i)(t - t_i) + o((t - t_i)^2)$. Mathematically, this implies that in the vicinity of t_i , $d(t)$ varies almost linearly, and while clearly visible in figure 4, this regime is much shorter than the convective stage found experimentally. This suggests that the experimentally observed behaviour must arise via mechanisms not included in our model, e.g. three-dimensional effects.

As mentioned in the Introduction, Cerretelli & Williamson (2003) argue that the anti-symmetric vorticity in the co-rotating frame is responsible for the radial advection of the vortices. It is important to note that this gives a complete description of the motion of the vortex centres only if the viscous drift is negligible. Our analysis shows that this holds only in the advective phase, which exists only for sufficiently high Re . In the oscillatory phase and the bifurcation phase, viscous drift cannot be ignored, and for low Re , the vortex motion is completely dominated by viscous drift.

4.4. Dynamics of anti-vortices

The extrema of vorticity that we have described hitherto are positive maxima that we interpreted as vortex centres. At low Re , no further vorticity extrema occur, but at higher Re , the vorticity field deforms sufficiently for other critical points to be created through bifurcations. We show here that at $Re = 1000$, local minima of positive vorticity, termed anti-vortices in § 2.2, can develop through cusp bifurcations as described in § 3.1. The generic case is relevant here, as there is no symmetry around the points where the bifurcations occurs. However, as the global vorticity field satisfies the symmetry (3.14), a bifurcation event at some (x_0, y_0) must be accompanied by an identical event at $(-x_0, -y_0)$ at the same time.

Figure 9 shows the trajectories of all critical points of vorticity at $Re = 1000$. In addition to the original vortex centres and the saddle point at the origin, two extremum/saddle pairs are created at $t = 35.8$ in cusp bifurcations $(c) \rightarrow (b) \rightarrow (a)$ in figure 1, and they are annihilated again at $t = 60.9$ in the reverse bifurcation. It follows from the analysis in § 3.1 that close to the bifurcation, the extremum and the saddle essentially move along the eigendirection e of the zero eigenvalue of the Hessian that defines the x -coordinate used in the analysis. The two points move in opposite directions, and their velocities go to infinity as the bifurcation is approached. Under the generic assumption that the azimuthal direction e_θ (see figure 3a) at the bifurcation point is not collinear with e , it follows that

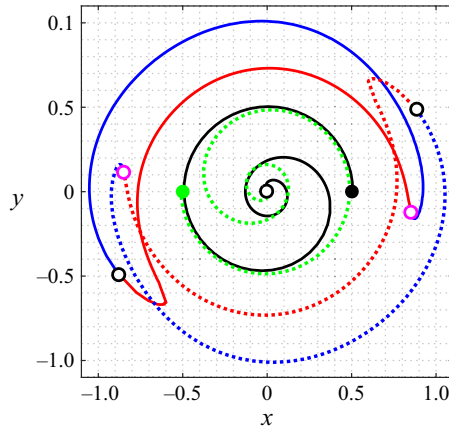


Figure 9. Trajectories of critical points of vorticity at $Re = 1000$. The black and dotted green curves are the trajectories of the vortices (local maxima), with the initial positions marked with filled circles. Red curves are anti-vortices (local minima), and blue curves are saddle points. Open circles mark bifurcations: purple for creation, and black for annihilation or vortex merging.

one of the critical points will rotate with the fluid flow in the anticlockwise direction, and the other will rotate against the flow, when sufficiently close to the bifurcation. Figure 9 shows that the saddle points rotate against the flow after the creation, but only for a very short time. As annihilation is approached, the anti-vortices exhibit the retrograde motion.

The annihilation process is illustrated in figure 10. Note that the bifurcations take place quite far from the origin. At the time of annihilation, the vorticity has been stretched out into filaments, and figure 10(a) shows that the anti-vortices and their corresponding saddles are present in the troughs between the filaments.

The anti-vortices continue to exist after the merging at $t = 55.6$ of the original vortices. Thus the axisymmetrisation of the single vortex left after merging is a topologically complex process, with an intermediate phase with two anti-vortices and two saddles.

Equations (3.11) predict that the distance d_{es} between an extremum and a saddle close to bifurcation follows a scaling of the form

$$d_{es}^2 = a_{es}t + b_{es}, \tag{4.12}$$

similar to (4.4), valid for the distance between the extrema in vortex merging. The fits shown in figure 11 confirm this theoretical prediction.

Recall that (2.15) showed that the strength of a positive vortex, measured by the value of vorticity at its centre, will decrease over the course of time. The same equation implies that, somewhat counter-intuitively, the opposite is the case for a positive anti-vortex. This is confirmed in figure 12, which shows that an anti-vortex increases its strength by six orders of magnitude between the creation at $t = 35.8$ and the destruction at $t = 60.9$. Nevertheless, the strength of the anti-vortex at the time of annihilation is 7.9×10^{-3} times the strength of the merged vortex at the origin, so it is still rather weak.

While the anti-vortices in the merging process considered here do not interact with the vortices, they may do so in flows that are more complex. In fact, it may be the saddles that are created together with anti-vortices in cusp bifurcations that have a physical significance. These saddles may merge with a true vortex in a subsequent cusp bifurcation, and hence remove that vortex from the flow. Bifurcations to that effect have been observed in a preliminary study of the vortex dynamics in the flow around a cylinder in a channel (Ozdemir 2023).

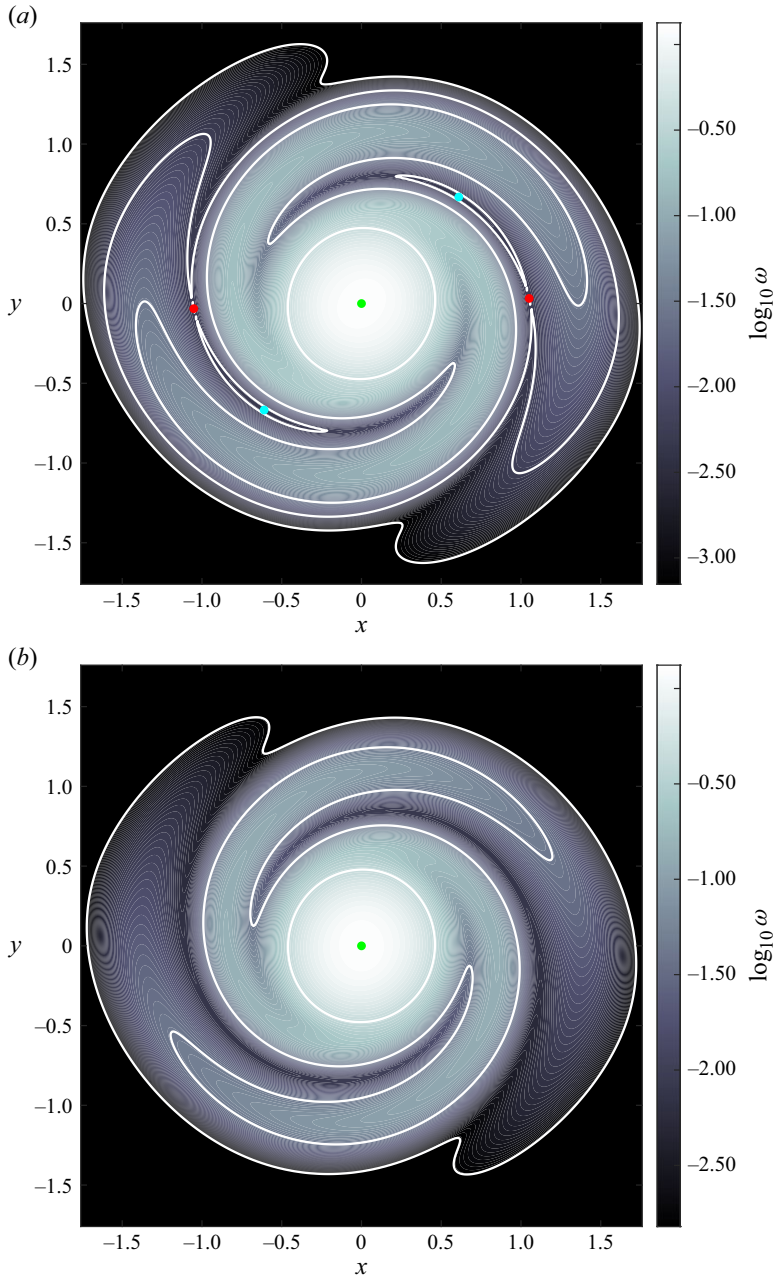


Figure 10. Snapshots of the vorticity field at $Re = 1000$: (a) just before anti-vortex annihilation at $t = 60.9$; (b) just after annihilation. The green point marks the merged vortex at the origin, cyan points are anti-vortices, and red points are saddles. Typical iso-vorticity curves are shown in white. In (a), the iso-vorticity curve through the saddle points is also shown. As $t \rightarrow 60.9$, the saddles and the corresponding anti-vortices approach each other.

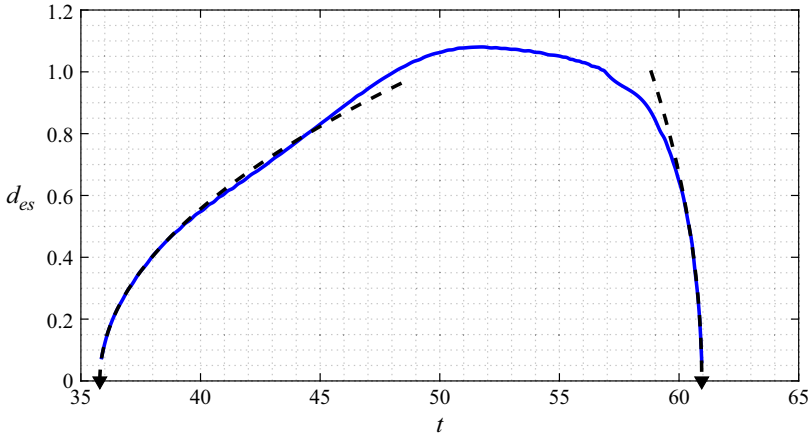


Figure 11. The distance d_{es} between the critical points in an anti-vortex/saddle pair at $Re = 1000$. Quadratic fits of the form (4.12) near the bifurcations are shown as dashed lines.

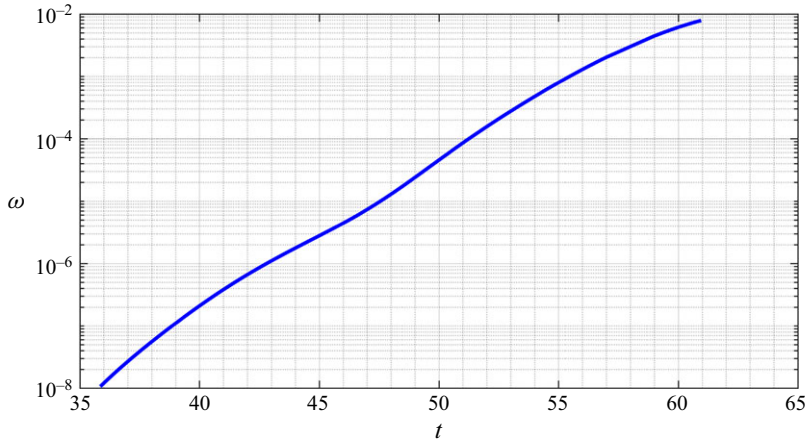


Figure 12. Development of the vorticity at an anti-vortex over its lifetime, at $Re = 1000$.

5. Conclusions

Keeping track of the critical points of vorticity ω is a simple way of understanding the fundamental features of the vortex dynamics of a two-dimensional fluid flow. Positive local maxima of ω (or negative minima) can be interpreted as vortex centres, and bifurcations of these points, with time as a parameter, indicate creation, annihilation or merging of vortices.

We have presented a general description of the dynamics of critical points of vorticity that decomposes their velocities into advection with the fluid and a drift proportional to viscosity. The viscous drift accounts for the influence of diffusion on the motion of the vortex centre. We give precise conditions, related to the local symmetry of the vorticity field, for the viscous drift to be zero or small. These conditions are violated close to a bifurcation, where the viscous drift velocity becomes unbounded and invariably dominates the motion.

Analysing the merging of two identical vortices in the light of the theory identifies low- Re and high- Re regimes, each consisting of temporal phases with a characteristic balance

between advection and viscous drift. This balance changes smoothly with time, and there do not seem to be specific physical events that instantaneously trigger the change from one phase into another. Only the merging time t_m is rigorously defined as a bifurcation point.

In addition to vortex centres as local maxima of positive vorticity, we have also identified anti-vortices in the form of local minima of positive vorticity. They appear in the troughs between the vorticity filaments that develop during vortex merging. They are created and annihilated together with a saddle point in cusp bifurcations. While the anti-vortices themselves may have limited physical importance, their companion saddles have the potential to interact with true vortices and annihilate them in cusp bifurcations. This may occur in more complex flows and is currently under investigation.

Declaration of interests. The authors report no conflict of interest.

REFERENCES

- ANDERSEN, M., SCHRECK, C., HANSEN, J.S. & BRØNS, M. 2019 Vorticity topology of vortex pair interactions at low Reynolds numbers. *Eur. J. Mech. (B/Fluids)* **74**, 58–67.
- BRANDT, L.K. & NOMURA, K.K. 2006 The physics of vortex merger: further insight. *Phys. Fluids* **18** (5), 051701.
- BRØNS, M. & BISGAARD, A.V. 2010 Topology of vortex creation in the cylinder wake. *Theor. Comput. Fluid Dyn.* **24** (1–4), 299–303.
- CERRETELLI, C. & WILLIAMSON, C.H.K. 2003 The physical mechanism for vortex merging. *J. Fluid Mech.* **475**, 41–77.
- DEEM, G. & ZABUSKY, N. 1978 Vortex waves: stationary ‘V states’, interactions, recurrence, and breaking. *Phys. Rev. Lett.* **40** (13), 859–862.
- DRITSCHEL, D.G. 1985 The stability and energetics of corotating uniform vortices. *J. Fluid Mech.* **157**, 95–134.
- DRITSCHEL, D.G. 1988 Contour surgery: a topological reconnection scheme for extended integrations using contour dynamics. *J. Comput. Phys.* **77** (1), 240–266.
- E, W. & LIU, J.-G. 1996a Finite difference schemes for incompressible flows in vorticity formulations. *ESIAM: Proceedings* **1**, 181–195.
- E, W. & LIU, J.-G. 1996b Vorticity boundary condition and related issues for finite difference schemes. *J. Comput. Phys.* **124** (2), 368–382.
- EATON, J.W., BATEMAN, D., HAUBERG, S. & WEHBRING, R. 2021 GNU Octave version 6.3.0 manual: a high-level interactive language for numerical computations. <https://docs.octave.org/octave-6.3.0.pdf>.
- HANSEN, J.S. 2011 *GNU Octave: Beginner’s Guide*. Packt Publishing. <https://www.packtpub.com/en-us/product/gnu-octave-beginners-guide-9781849513333>.
- HEIL, M., ROSSO, J., HAZEL, A.L. & BRØNS, M. 2017 Topological fluid mechanics of the formation of the Kármán-vortex street. *J. Fluid Mech.* **812**, 199–221.
- JING, F., KANSO, E. & NEWTON, P.K. 2012 Insights into symmetric and asymmetric vortex mergers using the core growth model. *Phys. Fluids* **24** (7), 073101.
- JOSSERAND, C. & ROSSI, M. 2007 The merging of two co-rotating vortices: a numerical study. *Eur. J. Mech. (B/Fluids)* **26** (6), 779–794.
- LE DIZÈS, S. & VERGA, A. 2002 Viscous interactions of two co-rotating vortices before merging. *J. Fluid Mech.* **467**, 389–410.
- LEWEKE, T., LE DIZÈS, S. & WILLIAMSON, C.H. 2016 Dynamics and instabilities of vortex pairs. *Annu. Rev. Fluid Mech.* **48** (1), 507–541.
- MEUNIER, P., EHRENSTEIN, U., LEWEKE, T. & ROSSI, M. 2002 A merging criterion for two-dimensional co-rotating vortices. *Phys. Fluids* **14** (8), 2757–2766.
- MEUNIER, P., LE DIZÈS, S. & LEWEKE, T. 2005 Physics of vortex merging. *C. R. Physique* **6** (4–5), 431–450.
- NIELSEN, A.R., ANDERSEN, M., HANSEN, J.S. & BRØNS, M. 2021 Topological bifurcations of vortex pair interactions. *J. Fluid Mech.* **917**, A11.
- NIELSEN, A.R., MATHARU, P.S. & BRØNS, M. 2022 Topological bifurcations in the transition from two single vortices to a pair and a single vortex in the periodic wake behind an oscillating cylinder. *J. Fluid Mech.* **940**, A22.
- OVERMAN, E.A. & ZABUSKY, N.J. 1982 Evolution and merger of isolated vortex structures. *Phys. Fluids* **25** (8), 1297–1305.

- OZDEMIR, I.R. 2023 Topological descriptions of vortex dynamics and interactions. *MSc Thesis*, Technical University of Denmark, Department of Applied Mathematics and Computer Science.
- SREEJITH, M. & ANIL, L.S. 2021 On the roles of antisymmetric vorticity and particles changing over in two-dimensional vortex merging problems. *AIP Adv.* **11** (8), 085121.